PHASE SPACE TOMOGRAPHY CONSTRAINED BY THE VLASOV–FOKKER–PLANCK EQUATION USING EOSD DIAGNOSTICS AT KARA

F. Donoso*, M. Brosi, E. Bründermann, M. Frank, S. Funkner, J. Gethmann, A.-S. Müller, G. Niehues, M. Reissig, P. Schreiber
Karlsruhe Institute of Technology, Karlsruhe, Germany

Abstract

This study presents the first experimental application of longitudinal phase space tomography constrained by the Vlasov–Fokker–Planck equation (VFPE) using electro-optical spectral decoding (EOSD) diagnostics at the Karlsruhe Research Accelerator (KARA). The EOSD measurements are modeled as the convolution of the system's impulse response with the charge density profile at the time of acquisition. Combining this model with the VFPE we formulate a partial differential equation-constrained optimization framework for the inverse tomography.

Using this framework, we successfully reconstruct the longitudinal phase space of the electron bunch across different dynamical regimes, ranging from the stable state to the onset of micro-bunching. From the reconstructed phase space, we derive macroscopic beam observables including the longitudinal bunch length, energy-spread related horizontal bunch size, and coherent synchrotron radiation (CSR) power. The reconstructed observables are validated against synchronized measurements from three independent diagnostics. Overall, the results demonstrate that the VFPE-constrained approach, combined with a detailed EOSD forward model, provides a physically consistent reconstruction of the phase space density dynamics from EOSD measurements.

INTRODUCTION

Following our previous work [1,2], we applied the longitudinal phase space reconstruction algorithm to electro-optical spectral decoding (EOSD) measurements acquired at the Karlsruhe Research Accelerator (KARA). This partial differential equation-constrained framework enforces physical consistency between the reconstructed initial density and its turn-by-turn evolution. As the EOSD modulation encodes the electric field induced by the bunch within the crystal rather than the direct charge profile, our forward model explicitly incorporates this interaction [3, 4]. The resulting continuous space-time formulation of the reconstruction problem is presented in Eq. (1).

This formulation seeks to reconstruct the complete phase space trajectory, generated from the initial phase space density ψ^*, that best fits the measured EOSD signals. The optimization minimizes the error between the computed phase retardations, $\Gamma(t_n)$, obtained from this trajectory at time, t_n, and the measured signals, $\bar{\Gamma}_n$ for $n = 1, \ldots, m$. The regularization term, $\lambda R(\psi)$, is incorporated to mitigate challenges such as noise in the measurement data and the ill-posed nature of the inverse problem. The temporal evolution of the phase space density, ψ, is strictly constrained by the Vlasov–Fokker–Planck equation (VFPE), where H represents the Hamiltonian of the system , q and p denote the canonical position and momentum coordinates, respectively, and β_d and D correspond to the damping and diffusion parameters [5]. Furthermore, $\rho(q,t)$ defines the bunch profile, which is determined by projecting the phase space density along the position axis. Finally, G maps the bunch profile to the expected phase retardation, modeling the EOSD response [3,4].

$$
\begin{aligned}
\min_{\psi^* \geq 0} \quad & \sum_{n=1}^{m} \|\Gamma(t_n) - \bar{\Gamma}_n\|^2 + \lambda R(\psi^*) \\
\text{s.t.} \quad & \frac{\partial \psi}{\partial t} + \frac{\partial H}{\partial p}\frac{\partial \psi}{\partial q} - \frac{\partial H}{\partial q}\frac{\partial \psi}{\partial p} = \beta_d \frac{\partial}{\partial p}(p\psi) + D\frac{\partial^2 \psi}{\partial p^2}, \\
& \rho(q,t) = \int \psi(q,p,t)\mathrm{d}p, \\
& \Gamma(t_n) = G\left(\rho(q,t_n)\right), \\
& \psi^* = \psi(q,p,t_1).
\end{aligned}
\tag{1}
$$

To solve Equation (1), the continuous variables are discretized. This is achieved by solving the VFPE through operator splitting on a discrete spatial grid, where time steps t_n correspond to single-turn revolutions of the electron bunch in the storage ring. The continuous two-dimensional phase space is transformed into a one-dimensional vector, indexed by s, allowing the differential operators to be linearized into transfer matrices. To integrate the diagnostic, the EOSD diagnostic is modeled as a linear time-invariant (LTI) system to allow the measurement process to be formulated computationally as a matrix-vector product, directly representing the convolution of the bunch profile with the system's impulse response. By combining these discrete dynamic and measurement operators, the continuous problem in Equation (1) is recast into the matrix-based optimization problem [2] shown in Eq. (2).

$$
\begin{aligned}
\min_{\psi^*} \quad & \|\tilde{\mathrm{G}}\psi - \mathbf{\Gamma}\|^2 + \lambda R(\psi) \\
\text{s.t.} \quad & \mathrm{M}(\psi(s,t_n)) = \mathrm{D}\cdot\mathrm{R_K}\cdot\mathrm{R_D}\cdot\mathrm{K}(\psi(s,t_n)), \\
& \tilde{\mathrm{G}} = \begin{pmatrix} \mathrm{G}\cdot\mathrm{W} \\ \mathrm{G}\cdot\mathrm{W}\cdot\mathrm{M}(\psi(s,t_1)) \\ \vdots \\ \mathrm{G}\cdot\mathrm{W}\cdot\Pi_{n=1}^{m-1}\mathrm{M}(\psi(s,t_n)) \end{pmatrix}
\end{aligned}
\tag{2}
$$

* felipe.donoso@kit.edu

In Eq. (2), $\tilde{\mathrm{G}}$ denotes the extended system matrix, built iteratively turn-by-turn. It combines G, the Toeplitz convolution matrix for the EOSD impulse response, W, the projection matrix from phase space to bunch profile, and M, the transfer matrix governing the turn-by-turn evolution of the phase space.

The transfer matrix M includes the physical effects acting on the bunch during one revolution. Here, $\mathrm{R_K}$ and $\mathrm{R_D}$ represent a RF kick and drift due to the external fields, D accounts for synchrotron radiation damping and diffusion, and K models the collective wake potential matrices. Since K depends on the bunch profile, M remains nonlinear through its dependence on the current phase space density $\psi(s, t_n)$. To handle this inherent non-linearity, we assume that the bunch profile varies negligibly between consecutive turns. The profile from the preceding step is therefore used as an approximation to compute the wake potential operator and the transfer matrix M for the current turn. The resulting least-squares optimization problem in Eq. (2) is then solved using the projected-restarted non-negative conjugate gradient method for the normal equations [6].

In this work, the discrete optimization problem defined in Eq. (2) is utilized to reconstruct the charge density in the longitudinal phase space directly from experimental EOSD data, $\mathbf{\Gamma}$. The remainder of this paper outlines the practical application of this method.

LONGITUDINAL BEAM DYNAMICS

As expressed in Eq. (1), the deterministic particle dynamics are governed by the Hamiltonian. Following [7], it is convenient to split H into contributions from the external fields and contributions from collective self-interaction effects, such that $H(q, p, t) = H_e(q, p, t) + H_c(q, t)$. These components are defined as:

$$H_e(q, p, t) = \frac{1}{2}(q^2 + p^2),$$
$$H_c(q, p, t) = \frac{e f_{\mathrm{rev}}}{\sigma_{\mathrm{E}} f_{s,0}} \int_q^\infty \int_{-\infty}^\infty \tilde{\rho}(f) Z(f) e^{i2\pi f q'} df dq'. \tag{3}$$

The unperturbed Hamiltonian, H_e, describes the standard harmonic synchrotron motion and depends on the dimensionless, generalized phase space coordinates $q = z/\sigma_{z,0}$ (normalized longitudinal position), $p = (\mathrm{E} - \mathrm{E}_0)/\sigma_{\mathrm{E},0}$ (normalized energy deviation), and $\theta = f_{s,0} t$. With these variables, the VFPE in Eq. (1) is written in generalized coordinates, with the time derivative and longitudinal damping scaled consistently as in [8]. Conversely, H_c models the non-linear self-interaction of the bunch. In this term, e is the electron charge, f_{rev} is the revolution frequency, $f_{s,0}$ is the nominal synchrotron frequency, and $\sigma_{\mathrm{E},0}$ is the natural energy spread. The integral captures the interaction between the bunch's frequency spectrum, $\tilde{\rho}(f)$, and the longitudinal impedance, $Z(f)$, which is the Fourier transform of the wake field and describes the frequency-domain response of the accelerator environment to the beam, including effects such as coherent synchrotron radiation (CSR) self-interaction [5, 9].

Consequently, the solution of the VFPE governs the time dynamics of the beam for a specific accelerator configuration. This configuration directly determines the operators used in Eq. (1) and consequently the transfer matrices of Eq. (2).

At the same time, this configuration establishes the physical limits of the bunch profile dimensions, and thus the phase space. It is crucial to emphasize that if the physical parameters defining the simulated accelerator model do not accurately correspond to the actual experimental conditions of the measured data, the phase space reconstruction is constrained by this mismatch, and the inverse problem may lead to biased or physically inconsistent phase spaces.

EXPERIMENTAL MEASUREMENTS

The experimental data for this study were acquired at the Karlsruhe Research Accelerator, a storage ring with a circumference of 110.4 m and an RF frequency of 500 MHz. During these measurements, the machine was configured for short-bunch operation at a beam energy of 1.3 GeV [10]. To validate the physical accuracy of the phase space reconstruction, we utilized synchronized turn-by-turn measurements from three complementary diagnostics [11]: the longitudinal bunch profile derived from EOSD measurements, the emitted coherent synchrotron radiation (CSR) power recorded by fast THz detectors, and the horizontal beam profile observed by a visible light monitor, used to determine the horizontal bunch size in a dispersive section as a proxy for the energy spread.

The core of our reconstruction relies on the electro-optical spectral decoding (EOSD) system. In this setup, an electro-optical crystal is installed in-vacuum close to the beam path [3, 4, 12]. As the electron bunch passes, its highly compressed Coulomb field modifies the intrinsic birefringence of the crystal via the Pockels effect [13]. A chirped laser pulse is sent through the crystal, and the induced change of birefringence causes a shift in the laser's polarization. Using waveplates and polarization optics, this polarization change is converted into an intensity modulation. The modulated laser pulse is then detected with a fast spectrometer based on a grating and the KALYPSO line-array detector [14, 15], enabling turn-by-turn single-shot measurements of the longitudinal bunch profile with sub-picosecond resolution [3, 4, 13].

The emitted CSR power is measured with fast THz detectors based on room-temperature zero-bias Schottky barrier diodes, which are sensitive to the coherent radiation emitted by the bunch in the THz range [16]. These detectors are read out with the KAPTURE data acquisition system [17], which enables bunch-by-bunch measurements of the CSR intensity.

The horizontal bunch profile is detected via turn-by-turn measurements of the synchrotron radiation at the Visible Light Diagnostics port [18], located in a dispersive section of the storage ring, using the fast line array detector KALYPSO [19]. Because the horizontal bunch size is correlated with the energy spread through the dispersion, the emittance, and the beta function, variations in the measured horizontal

profile are used here as an indicator for changes in the energy spread.

The synchronized diagnostics measurements allow a direct comparison of the reconstructed longitudinal phase space with independent observables of the beam dynamics [11, 20]. For example, the synchronized data reveal that the appearance of micro-bunching substructures on the EOSD profile coincides directly with intense bursts of emitted CSR power [9, 21]. Furthermore, during these burst phases, the diagnostics record an expected simultaneous increase in both the overall longitudinal bunch length and the horizontal bunch size (energy spread), followed by a damping phase once the substructures wash out [11, 21].

RESULTS

The results presented were obtained from 3,500 consecutive runs of the phase space reconstruction algorithm defined in Eq. (2). Each run of the iterative algorithm [2] is initialized with a 2D Gaussian phase space distribution and utilizes 130 consecutive EOSD measurements, corresponding to half of a synchrotron period. The complete sequence of experimental EOSD measurements used for the reconstructions is displayed as a sinogram in Fig. 1 (labeled as 'longitudinal profile'). Figure 2 illustrates two exemplary phase space reconstructions: one at turn 24,000, representing a stable regime prior to the onset of micro-bunching, and another at turn 27,000, where the micro-bunching instability is fully active and phase space substructures are clearly visible [5, 9].

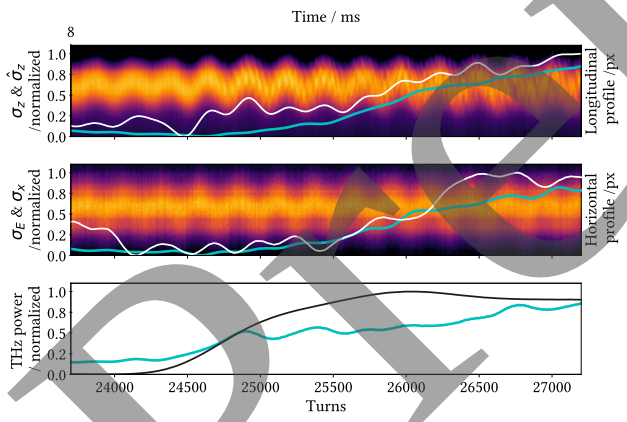

Figure 1: Synchronized measurements and reconstructed observables. Top: EOSD sinogram with measured bunch length $\hat{\sigma}_z$ (white) and reconstructed bunch length (cyan). Middle: Horizontal profile with measured horizontal bunch size σ_x (white) and reconstructed energy spread (cyan). Bottom: THz power signal (black), and reconstructed CSR power (cyan). All curves were smoothed with the same moving-average filter.

To validate the physical accuracy of the reconstructions, the macroscopic beam parameters extracted from the reconstructed phase space densities are compared against independent, synchronized diagnostic measurements. Specifically, we utilize the estimations for the longitudinal bunch length ($\hat{\sigma}_z$), the horizontal bunch size (σ_x), and the THz power as derived in the prior work by Brosi *et al.* [10]. As shown in Fig. 1, the beam quantities calculated directly from the reconstructed phase space exhibit a high degree of agreement with these independent experimental measurements.

It is important to note that the horizontal bunch size (σ_x) is formally related to the energy spread (σ_E) via the dispersion function, as detailed in [20]; however, for the dynamics observed here, they can be assumed to be directly proportional. Furthermore, the macroscopic parameters σ_z and σ_E from our reconstruction are determined by fitting a Gaussian function to the 1D projections of the reconstructed phase space onto the position and energy deviation axes, respectively, rather than computing the root-mean-square (RMS) directly. This approach is necessary because the reconstructed phase space exhibits a residual background noise ring (visible in Fig. 2). A direct RMS calculation would be disproportionately skewed by this peripheral noise, artificially inflating the apparent bunch length and energy spread. This reconstruction artifact originates from slight mismatches between our theoretical impulse response model of the EOSD system and the true experimental response [4].

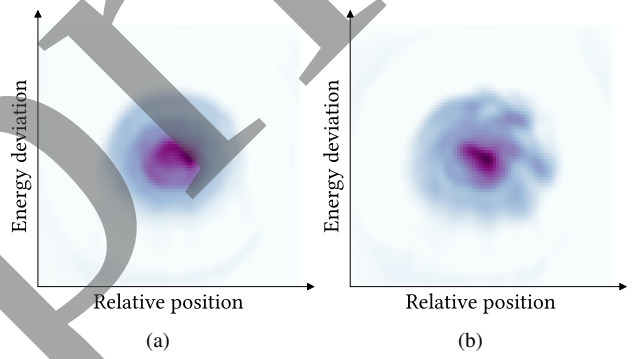

Figure 2: Reconstructed phase space density at (a) turn 24000, showing a smooth distribution without visible micro-bunching, and (b) turn 27000, showing pronounced micro-bunching structures associated with stronger CSR emission; the color gradient indicates local density, with lighter colors corresponding to lower values.

CONCLUSION

The results presented show that VFPE-constrained tomography, combined with an EOSD forward model, provides a physically consistent reconstruction of the longitudinal phase space at KARA. The good agreement between reconstructed quantities and independent synchronized measurements confirms that the underlying VFPE model, implemented in Inovesa [22], captures the essential beam dynamics from stable operation to the onset of micro-bunching. This provides an experimental validation of both the inverse reconstruction method and the forward beam-dynamics solver. These results establish a basis for future physics-informed prediction, inverse modeling, and beam control in storage rings.

ACKNOWLEDGEMENTS

F.D. gratefully acknowledges support from the MathSEE PhD Bridge Program and KCDS.

REFERENCES

[1] F. Donoso *et al.*, "Longitudinal phase space density tomography constrained by the Vlasov-Fokker-Planck equation", in *Proc. IPAC'24*, Nashville, TN, USA, May 2024, pp. 2350–2353. doi:10.18429/JACoW-IPAC2024-WEPG55

[2] F. Donoso *et al.*, "Extended phase space tomography for eosd simulation considering crystal geometry effects", in *Proc. IPAC'25*, Taipei, Taiwan, Jun. 2025, pp. 2818–2821. doi:10.18429/JACoW-IPAC2025-THPM063

[3] M. Reissig *et al.*, "Development of an Electro-Optical Longitudinal Bunch Profile Monitor at KARA Towards a Beam Diagnostics Tool for FCC-ee", in *Proc. IPAC'22*, Bangkok, Thailand, May 2022, pp. 296–299. doi:10.18429/JACoW-IPAC2022-MOPOPT025

[4] M. Reissig *et al.*, "Simulations of an electro-optical in-vacuum bunch profile monitor and measurements at KARA for use in the FCC-ee", in *Proc. IPAC'24*, Nashville, TN, USA, May 2024, pp. 2354–2357. doi:10.18429/JACoW-IPAC2024-WEPG56

[5] T. Boltz *et al.*, On the Perturbation of Synchrotron Motion in the Micro-Bunching Instability, 2022, doi:10.48550/ARXIV.2211.15086

[6] S. Gazzola, P. C. Hansen, and J. G. Nagy, "IR Tools: a MATLAB package of iterative regularization methods and large-scale test problems", *Numer. Algor.*, vol. 81, no. 3, pp. 773–811, 2019. doi:10.1007/s11075-018-0570-7

[7] R. L. Warnock and J. A. Ellison, "A General Method for Propagation of the Phase Space Distribution, with Application to the Sawtooth Instability", 2000. doi:10.2172/753322

[8] P. Schönfeldt, "Simulation and measurement of the dynamics of ultra-short electron bunch profiles for the generation of coherent THz radiation", 2018. doi:10.5445/IR/1000084466

[9] M. Brosi *et al.*, "Studies of the Micro-Bunching Instability in the Presence of a Damping Wiggler", *J. Phys. Conf. Ser.*, vol. 1067, p. 062017, 2018. doi:10.1088/1742-6596/1067/6/062017

[10] M. Brosi *et al.*, "Synchronous Measurements of Electron Bunches Under the Influence of the Microbunching Instability", in *Proc. IPAC'19*, Melbourne, Australia, May 2019, pp. 3119–3122. doi:10.18429/JACoW-IPAC2019-WEPTS015

[11] M. Brosi, "Overview of the Micro-Bunching Instability in Electron Storage Rings and Evolving Diagnostics", in *Proc. IPAC'21*, Campinas, SP, Brazil, May 2021, pp. 3686–3691. doi:10.18429/JACoW-IPAC2021-THXA02

[12] M. Reissig *et al.*, "First two-bunch measurements using the electro-optical near-field monitor at KARA", in *Proc. IPAC'23*, Venice, Italy, May 2023, pp. 4756–4759. doi:10.18429/JACoW-IPAC2023-THPL121

[13] S. Casalbuoni, H. Schlarb, B. Schmidt, P. Schmüser, B. Steffen, and A. Winter, "Numerical studies on the electro-optic detection of femtosecond electron bunches", *Phys. Rev. Spec. Top. Accel. Beams*, vol. 11, no. 7, p. 072802, 2008. doi:10.1103/PhysRevSTAB.11.072802

[14] L. Rota *et al.*, "KALYPSO: A Mfps Linear Array Detector for Visible to NIR Radiation", *Proceedings of the 5th Int. Beam Instrumentation Conf.*, vol. IBIC2016, 4 pages, 1.276 MB, 2017. doi:10.18429/JACoW-IBIC2016-WEPG46

[15] C. Gerth, M. Caselle, D. R. Makowski, A. Mielczarek, L. Rota, and B. Steffen, "KALYPSO: Linear Array Detector with Continuous Read-Out at MHz Frame Rates", in *Proc. IBIC'19*, Malmö, Sweden, Sep. 2019, pp. 271–274. doi:10.18429/JACoW-IBIC2019-TUPP001

[16] J. L. Steinmann *et al.*, "Continuous bunch-by-bunch spectroscopic investigation of the microbunching instability", *Phys. Rev. Accel. Beams*, vol. 21, no. 11, p. 110705, 2018. doi:10.1103/PhysRevAccelBeams.21.110705

[17] M. Caselle *et al.*, "KAPTURE-2. A picosecond sampling system for individual THz pulses with high repetition rate", *J. Instrum.*, vol. 12, no. 01, p. C01040, 2017. doi:10.1088/1748-0221/12/01/C01040

[18] B. Kehrer *et al.*, "Visible Light Diagnostics at the ANKA Storage Ring", in *Proc. IPAC'15*, Richmond, VA, USA, May 2015, pp. 866–868. doi:10.18429/JACoW-IPAC2015-MOPHA037

[19] B. Kehrer *et al.*, "Turn-by-Turn Horizontal Bunch Size and Energy Spread Studies at KARA", in *Proc. IPAC'19*, Melbourne, Australia, May 2019, pp. 2498–2500. doi:10.18429/JACoW-IPAC2019-WEPGW016

[20] B. Kehrer *et al.*, "Synchronous detection of longitudinal and transverse bunch signals at a storage ring", *Phys. Rev. Accel. Beams*, vol. 21, no. 10, p. 102803, 2018. doi:10.1103/PhysRevAccelBeams.21.102803

[21] B. Kehrer *et al.*, "Time-Resolved Energy Spread Studies at the ANKA Storage Ring", in *Proc. IPAC'17*, Copenhagen, Denmark, May 2017, pp. 53–56. doi:10.18429/JACoW-IPAC2017-MOOCB1

[22] P. Schönfeldt, M. Brosi, M. Schwarz, J. L. Steinmann, and A.-S. Müller, "Parallelized Vlasov-Fokker-Planck solver for desktop personal computers", *Phys. Rev. Accel. Beams*, vol. 20, no. 3, p. 030704, 2017. doi:10.1103/PhysRevAccelBeams.20.030704